Antiproton-Initiated LiH Plasma Generated in a Penning Trap

K. J. Meyer[†], D. P. Coughlin[††], K. J. Kramer[†††], and G. A. Smith
Propulsion Engineering Research Center
Penn State University
19 Research East, University Park, PA 16802
kjm155@psu.edu, (256) 863-6070

[†] *NASA GSRP Student, Department of Aerospace Engineering*
[††] *Boeing Graduate Fellow, Department of Aerospace Engineering*
[†††] *NASA GSRP Student, Department of Mechanical Engineering*

Abstract. Antimatter annihilation is one of few propulsion concepts able to provide near-interstellar speeds for spacecraft. It is also one of the least developed propulsion concepts, as it suffers from several technological challenges. However, with the High Performance Antimatter Trap (HiPAT) constructed at Marshall Space Flight Center, we can begin first-stage propulsion demonstrations with only 5 x 10^9 antiprotons. Here, we consider a prototype of an antimatter-initiated lithium hydride (LiH) plasma thruster. Unlike arc jets, PPT thrusters, and other electric propulsion devices that use an external current to create and drive a hot plasma, an antimatter-initiated LiH plasma is heated by a microfission process of antiprotons annihilating with a thin uranium shell. Through the use of the MHD code MACH2, we investigate the expansion and expulsion of such LiH plasmas using magnetic confinement.

INTRODUCTION

A desirable specific impulse (I_{sp}) for a precursor interstellar mission is roughly 10^5 sec. Chemical propulsion can only provide up to I_{sp} ~ 500 sec.[1] Of the other several advanced propulsion techniques – electric, fusion, laser/solar momentum, and antimatter – only fusion, laser lightsails, and antimatter can conceivably provide near-interstellar speeds.

Fusion propulsion such as inertial electrostatic confinement (IEC) and magnetized target fusion (MTF) can provide specific impulses beyond 120,000 sec.[2] However, most tokamaks and spheromaks that produce the fusion plasmas are quite massive, and are currently too unstable to provide a sufficient output energy greater than input. Laser lightcraft, which do not use propellant but laser energy to attain high Δv, require tremendous pointing accuracy between the planet-based laser and an essentially weightless spacecraft.

Beamed core antimatter propulsion offers the highest specific impulse known in existence, 10^7 sec. Direct reaction of a proton and antiproton and expulsion of its immediate products accomplish this.[3] A drawback is an extremely low thrust, which places a stiff minimum requirement of kilograms of antiprotons in order to propel a space probe to near-interstellar speeds.[4] An alternative plasma core antimatter engine design would require 1-10 grams of antiprotons, but this is still enormously higher than the world's current production level of 14 ng per year.

In previous papers, we have devised hybrid concepts that reduce antiproton requirements down to 1-100 μg. One such example is Antiproton-Catalyzed Microfission/fusion, which is useful for interplanetary missions (ICAN).[5] Another

example is Antimatter-Initiated Microfusion (AIM)[6], a synergy of antimatter and nuclear fusion technologies. This concept is used in tandem with the AIMStar project, of which its mission is to deliver a 240 kg payload to the Oort Cloud within 50 years.[7] AIMStar requires only 28.5 μg of antiprotons.

The AIM process begins with the injection of 10^{11} antiprotons into a Penning reaction trap that is roughly 0.5 cm in diameter. The double-nested potential well of depth 10 kV in the reaction region splits the beam of antiprotons into two clouds of approximately equal density. Fusion fuel droplets such as DHe^3 or DT enter the reaction region juxtaposing the two clouds. These 42 ng droplets are coated with a thin layer of U^{238}, so that collapsing the two antiproton clouds upon the fuel target will annihilate 5 x 10^9 antiprotons through a microfission process. The fission fragments heat the fuel core, fully ionizing the target components at a temperature of ~10 eV. After increasing the well to 600 kV, it produces an ion temperature of 100 keV and density $6x10^{17}$ ions/cm^3. This satisfies the Lawson criterion for a full fusion burn.[6]

Antiproton production scales with demand and can be augmented when seen fit. The demand ultimately depends on current storage and transportation capabilities of the antiprotons. The two portable, high-density antiproton traps that are in existence today – the Penn State antimatter trap (Mark I) and NASA Marshall Space Flight Center's High Performance Antimatter Trap (HiPAT) – can store quantities of 10^9 and 10^{12} antiprotons, respectively.

Because only 5 x 10^9 antiprotons are required per shot of fusion fuel, smaller-scale experiments may be conducted. We have proposed a first-generation antimatter thruster that serves as a predecessor to AIM. The thruster uses a combination of HiPAT and a scaled version of the AIM reaction trap. This reaction trap allows quick storage of 5 x 10^9 antiprotons, with lithium hydride fuel droplets as fusion simulants. Similarities to the AIM paradigm include a double-nested potential well and antiproton microfission with a U^{238} shell. The fission fragments ionize the LiH target, which expands and propels through a magnetic configuration. The MHD program MACH2 is therefore used to confirm the plasma confinement and propulsion at varying magnetic field strengths.

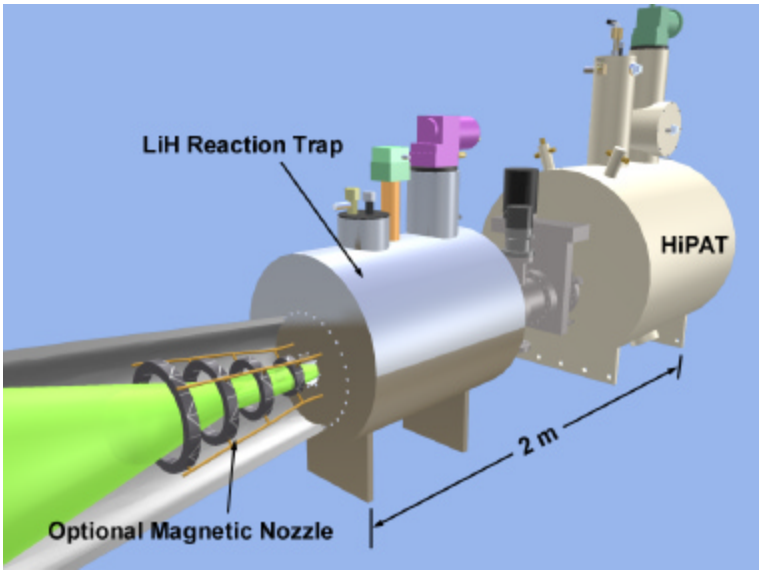

Figure 1. HiPAT and reaction trap assembly.

LIH HEATING WITH ANTIPROTONS

We consider HiPAT as an optimum choice for a LiH plasma experiment due to its proficiency in storage quantities and lifetimes. HiPAT is a Penning-Malmberg trap with a solenoid super-conducting magnet and a series of electrodes that confine a set of charged particles. The Brillouin limit, given as[8]

$$N_B = \frac{B^2}{8\pi m_p c^2} V(cm^3), \tag{1}$$

suggests that approximately 10^{12} antiprotons may be stored with a maximum HiPAT magnetic field of 4 T and control volume of 850 cm^3. The space-charge limit, governed by Coulomb's Law, predicts that the end potentials must be maintained above 10 kV. HiPAT can provide a potential of 20 kV.

The electric potential helps govern characteristic lifetimes within the trap, particularly with the antiproton axial frequency. Scattering collisions of antiprotons with background gas is one significant loss mechanism. This radial diffusion half-life is given by the formula

$$\left(t_{1/2}\right)_{dif} = \frac{1}{n\sigma v} \cdot \left(\frac{\omega_c}{\omega_z}\right)^2, \tag{2}$$

where axial frequency ω_z = 4.6 MHz (V_o = 20 kV) and cyclotron frequency ω_c = 383 MHz. The collision frequency $n\sigma v$ is dominated by ion-background and ion-ion collisions at low temperatures. When considering background gas hydrogen, the collision frequency is approximately 15 μs^{-1} at 10^{-11} torr. This gives a scattering half life of ~ 500 days. The other loss mechanism, direct background annihilation, depends on the energy of the antiprotons.[9] An antiproton storage energy of 100 eV permits lifetimes in excess of one year.

We assume that approximately 10^{12} antiprotons are loaded into HiPAT at a national particle accelerator/decelerator lab (e.g. Fermi National Laboratory, Brookhaven National Laboratory). These antiprotons sympathetically cool to 100 eV with electrons already residing in the trap. The portable trap mates with a reaction trap (Figure 1) at another research site. By electrostatic means the antiprotons are transferred in order to guarantee that 5 x 10^9 antiprotons reside in the LiH reaction trap.

Smaller confinement quantities and shorter time scales relax the conditions for the reaction trap. To allow proper expansion of the LiH plasma, we assume that the control region is similar to HiPAT, with r_o = 3 cm, and l = 30 cm. A 2 T axial magnetic field can be provided using permanent, rare earth magnets, or a superconducting coil. The reaction trap consists of approximately eleven electrodes, two of which are not shown in Figure 2, used for detection. These electrodes would provide a double-nested potential well, which splits the initial packet of antiprotons into two clouds of approximate equal density. The reaction trap also contains a portal, which introduces the LiH fuel droplet into the control region.

The 100 ng fuel droplet consists of a 22.5 μm LiH core (40 ng), surrounded by a U^{238} shell of ~0.5 μm thickness. When the antiproton cloud is collapsed upon the fuel pellet, the antiprotons immediately annihilate with the uranium shell. Pions and gamma rays spark microfission with the U^{238} nucleus. This produces two fission fragments of approximate mass 111 a.u. of 100 MeV each. Over the span of 23 μm, the energy is

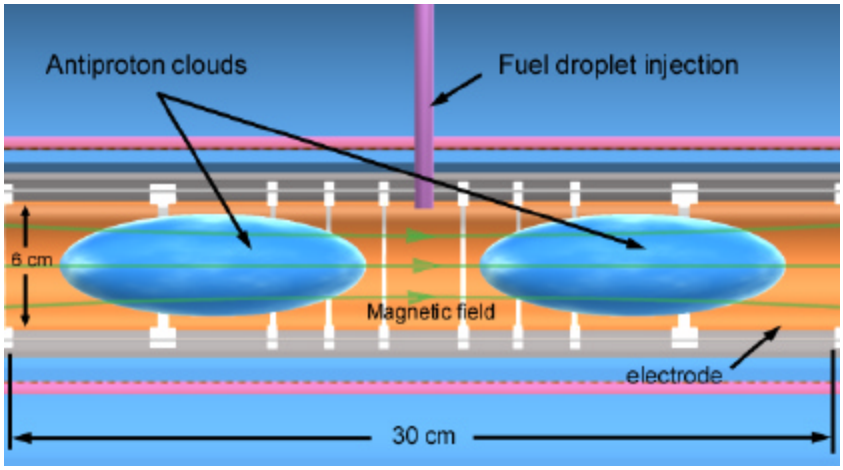

Figure 2. Cross-section of the LiH Penning-Malmberg control volume.

deposited into the remaining uranium shell and/or the LiH core.

Figure 3 describes the deposition energy per 0.5 micron layer of the fuel droplet. The values were derived from a 3-D Monte Carlo simulation that assumes instantaneous impact of all 5 x 10^9 antiprotons.[10] The average specific internal energy of the LiH is 0.244 J/kg. This correlates to an initial temperature of approximately 10 eV, which is above the first ionization state for lithium.

In reality, ablation of the uranium shell before all 5 x 10^9 antiprotons annihilate is a distinct issue, and it suggests increasing the uranium shell thickness. For simulation purposes, however, the uranium shell is neglected.

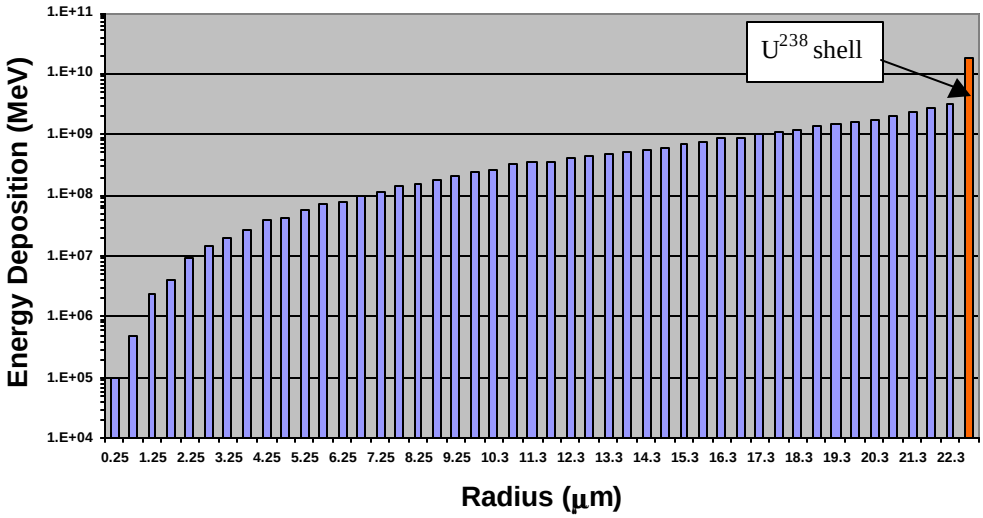

Figure 3. Energy deposition vs. radius for 23 um LiH droplet.

ASSUMPTIONS OF THE LIH PLASMA

Because we are dealing with a neutral, collisional plasma, MACH2 can provide a robust numerical solution to the 2-D axis-symmetric problem.[11] However, there are certain limitations with this code, particularly for an unsteady expansion. Also, certain parameters of the MHD equations can be neglected due to the initial temperature and density of the LiH gas.

An immediate restriction to the MACH2 code involves the inability to implement

spherical geometry. The initial mesh must be discretized into quadrilateral blocks. Therefore, the initial blocks containing the LiH resemble that of a "cylinder", which resolves to a spherical expansion as time progresses. Second, only one species can be implemented per block. Here, we choose Li^+, since the initial temperature is less than the ionization temperature for hydrogen (13.6 eV), but greater than the first ionization potential for lithium (5.4 eV). Last, because MACH2 uses the MHD equations, it cannot model E fields. Therefore, we assume that the electric potential within the Penning-Malmberg region is immediately switched off after annihilation.

The ability to confine and electromagnetically influence plasma depends on two conditions. The first involves the beta ratio

$$\beta = \frac{p}{B^2/2\mu_o} \cong \frac{3knT/2}{B^2/2\mu_o}. \tag{3}$$

For $\beta > 1$ the kinetic pressure exceeds magnetic pressure, and the plasma is no longer confineable.[12] Using a temperature of 10 eV, the condition becomes

$$\frac{n(cm^{-3})}{B^2} < 1.7\times10^{17}. \tag{4}$$

The other criterion states that the Larmor (cyclotron) radius of the individual electron and the ion must be less than the mean free path for that species.[13,14] Using the formula for mean free path, the condition for electrons or ions to remain attached to B fields is

$$\frac{m_{i,e}v_\perp}{eB} < \frac{4.5\times10^{11}T^2}{n(cm^{-3})\ln\Lambda}, \tag{5}$$

with T specified in eV. When assuming that $v_\perp \approx \sqrt{kT/m_{i,e}}$, the conditions for ions and electrons become

$$\frac{n(cm^{-3})}{B} < 4.4\times10^{15} \qquad \text{(ions)} \tag{6}$$

and

$$\frac{n(cm^{-3})}{B} < 1.6\times10^{18}. \qquad \text{(electrons)} \tag{7}$$

Consider a Li^+ droplet with initial ρ = 0.79 g/cm^3 (n = 6.85 x 10^{22} cm^{-3}), the density of liquid LiH. External magnetic influences do not occur at this density, since B typically cannot exceed the current technological limit of ~ 10 Tesla. For initial MACH2 runs, we begin the expansion at 0.3-0.6 cm radius (n ~ 10^{15} cm^{-3}), so that the cell sizes of the mesh are computationally optimized. To maintain a stable code, we reduce the magnetic field to 0.2 T. This permits a spherical initial condition of the plasma at 0.6 cm, and it is sufficient for confinement.

The remaining assumptions pertain to parameters of the MHD equations. Thermal radiation can be neglected from our model because 1) bremsstrahlung and synchotron power loss formulae scale with n, which is small here; and 2) the initial temperature is only 10 eV. The Hall effect can also be ignored, since the condition

$$\left(\frac{\nu_i}{\omega_{ci}\ell_\perp}\right) << 1 \tag{8}$$

is valid for B > 0.1 T, as ω_{ci} is the ion cyclotron frequency.[12] Magnetic diffusion, however, must be included with the model since the magnetic Reynolds number

$$R_M = m_o v_o L / \eta \tag{9}$$

yields a value of ~ 10 for the initial droplet. Therefore, magnetic field lines are not frozen into this particular model. The most speculative model is thermal diffusion. Because a magnetically-confined plasma is "trapped" by vacuum, we presently neglect thermal diffusion when applying external magnetic fields.

RESULTS FROM MACH2 SIMULATIONS

Without a magnetic field, we expect the Li^+ plasma to behave similarly to Poiseuille flow with an abnormal initial condition. For example, the fluid expands to the wall and then propagates downstream, due to internal pressure. Such is evident in Figure 4. Here, the fluid diffuses throughout the entire control volume prior to its ejection downstream at an axial velocity of ~ 40000 m/s. This produces an undesired effect of heat transfer to the titanium or copper electrodes, which reduces the specific impulse and therefore thrust of the system.

Figure 5 illustrates results from a MACH2 simulation that is nearly exact to the one used for Figure 4, but with three discrepancies: 1) An axial magnetic field with B = 0.2 T is applied, based upon the conditions of Eqs. (4),(6), and (7); 2) Thermal diffusion is neglected; and 3) The density of the background is increased only to sufficiently accommodate for magnetic diffusion throughout the control volume. As expected, the plasma remains confined to the z-axis (axis of symmetry) and propagates downstream at a higher density of 3 x 10^{-6} kg/m^3, approximately a factor of 100 greater than without a magnetic field. Moreover, the axial velocity increases marginally to ~55000 m/s (local Mach number = 4), presumably due to the plasma's preferential expansion in the axial direction. Inclusion of the thermal diffusion model does not alter the specific impulse.

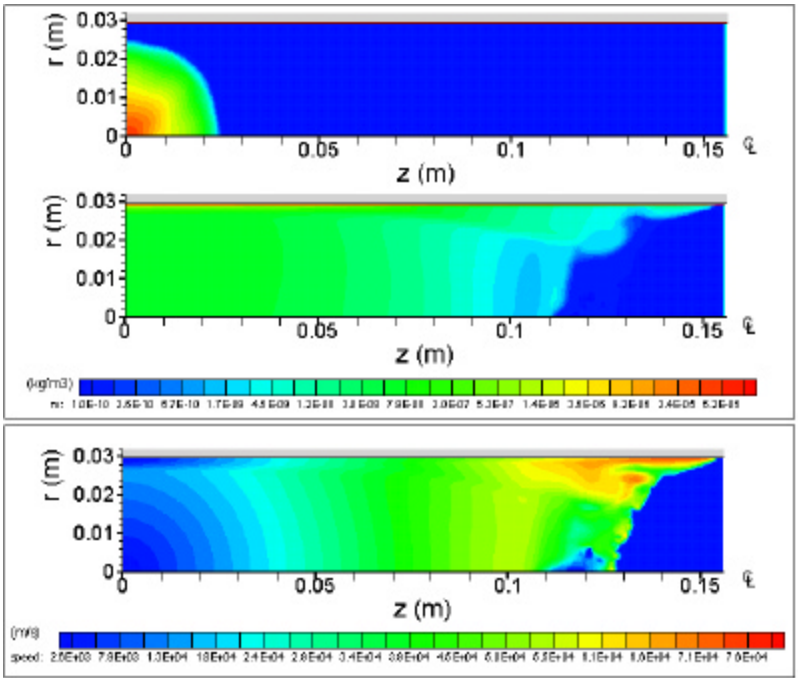

Figure 4. Contours of Li^+ expansion with B = 0.0 T, $\rho_o \sim 1x10^{-4}$ kg m^{-3}, and T_o = 10 eV. Density contours are shown at 0.3 μs and 2 μs, and speed contour is shown at 2 μsec.

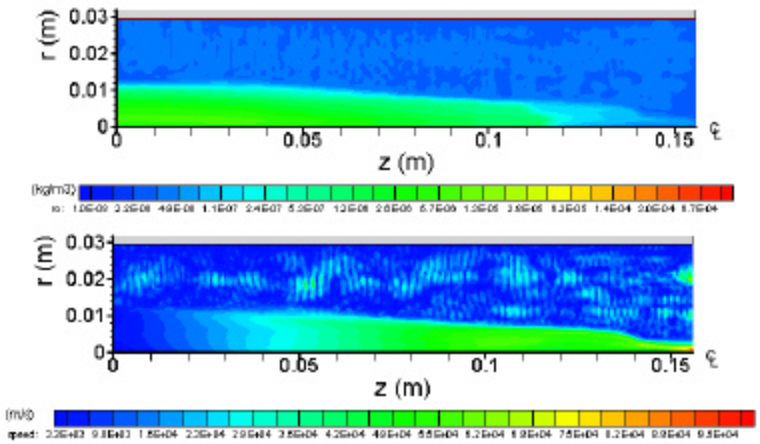

Figure 5. Density and speed contours of Li^+ expansion at 2 μsec with B = 0.2 T, $\rho_o \sim 1x10^{-4}$ kg m^{-3}, and T_o = 10 eV.

More recent studies involved B = 1.0 T, where the initial droplet was shrunk to 0.06 cm in order to satisfy the confinement conditions. Simulations ran extremely slow, due to the smaller cell sizes for such a mesh. Results as 1 μsec show that the plasma has flattened to a value no greater than 0.3 cm in radius, suggesting that the ion Larmor radius $r_L = m_i \, v_\perp / eB$, or ~ 0.1 cm, does plays a role with the radial extent of the plasma.

Because the dissociated hydrogen from LiH was not included in the simulation, we can speculate that the hydrogen would disperse in a situation similar to Li^+ w/o magnetic fields. Consequently, combinations of the above simulations can provide a basic illustration for both species of particles. Regardless, the density contours are dominated by the Li^+ propagation along the central axis of the trap.

To examine detachment of the 0.2 T-confined plasma, we extend the mesh beyond the trap boundaries. The flow speed is already supersonic, therefore requiring no converging magnetic fields typical of a converging nozzle. Rather, we only examine the divergent field lines typically present at the exit of a magnetic solenoid. At locations 5 cm from the exit and beyond, the majority of the poloidal magnetic field lines from the superconducting magnet have looped back to the opposite end of the apparatus. At 10 cm from the exit, the magnetic strength is approximately 0.01 T.

Figure 6 shows material contours at 4, 9, and 14 μsec, where values approaching "1" designate Li^+. Temperatures in the exhaust region approach 3 eV, which still implies a high degree of ionization. Initially, the plasma detaches from the magnetic field lines, but exhibits signs of weakening after 14 μsec. This is strong evidence that detachment is not due to recombination of ions and electrons, but due to violation of Eqs. (4) and (6). Indeed, as the plasma continues to expand, number density n also decreases, favoring attachment. The plume can detach at locations farther downstream, but will have unfortunately acquired some radial velocity component. Axial velocities recede to 45,000 m/sec, suggesting a nozzle efficiency of at least 82%.

CONCLUDING REMARKS

Presuming that a thrust-measuring device can be located sufficiently close to the exit of the trap, nozzle inefficiencies do not come into play. The specific impulse of the antiproton-initiated LiH plasma is 5800 sec, including a 10% uncertainty due to

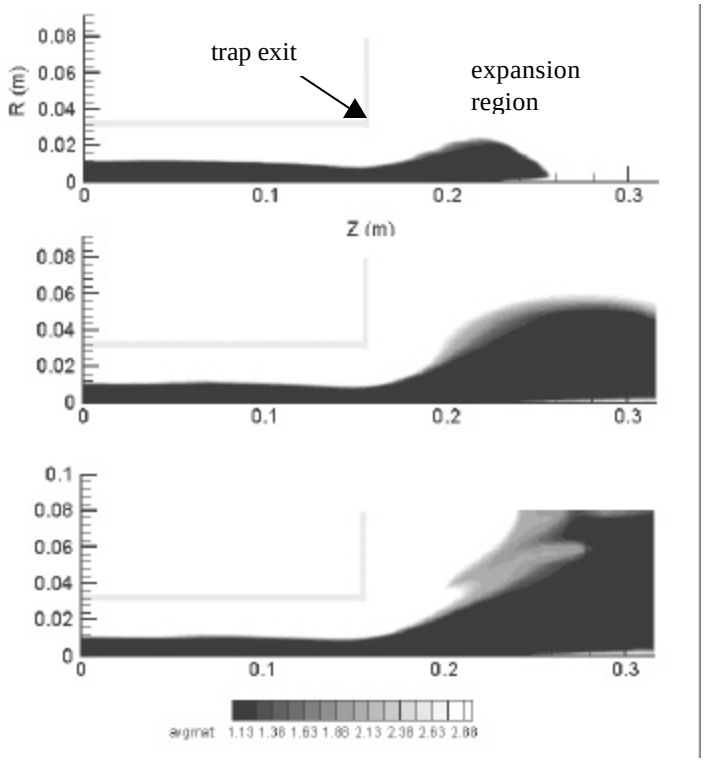

Figure 6. Contours of Li^+ expansion with B = 0.2 T through poloidal magnetic nozzle. Average material contours are shown at 4.0, 9.0, and 14 μsec.

bremsstrahlung radiation. Extrapolations of mass density (Figure 7) show that the LiH reaches background density (10^{18} m^{-3}) in 37 μsec. Therefore, a 20 ng pulse yields an average thrust of 35 mN. The other 20 ng component of the LiH harmlessly deflects off a gate valve in the opposite direction.

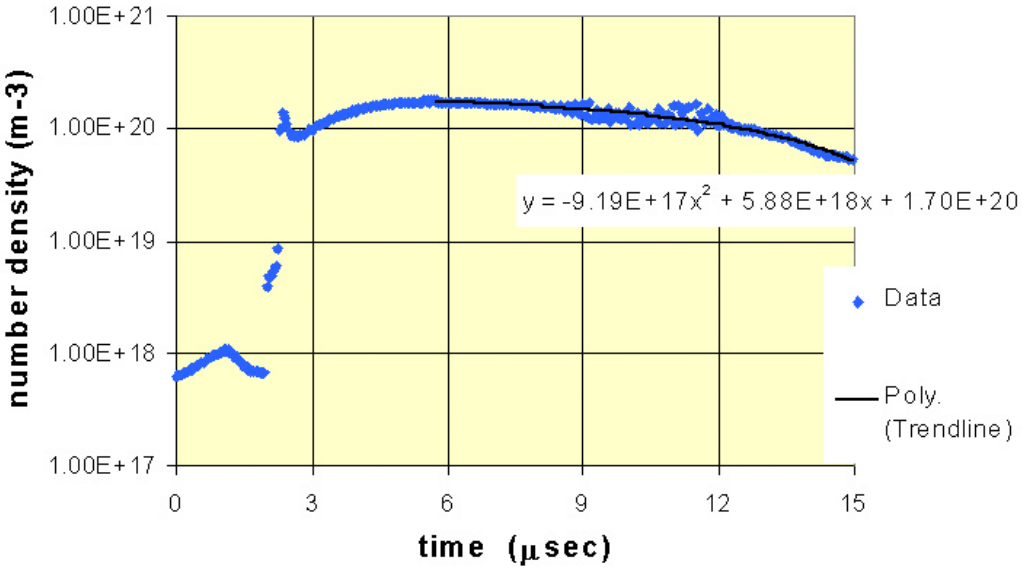

Figure 7. Comparison of number density over time at location Z = 15 cm, R = 0 cm, for B = 0.2 T Li+ plasma. The trendline yields a value of 10^{18} at 37 μsec.

The thrust and specific impulse can be measured with devices also used for ion engines and other electric propulsion devices that operate at low input power. Such an experiment with LiH plasma may be conducted upon further development of antiproton storage traps such as HiPAT, which will store 10^{12} antiprotons. It becomes imperative to develop storage traps in excess of 10^{12} antiprotons to promote use of antimatter in future propulsion technologies.

ACKNOWLEDGEMENTS

This research was sponsored by the NASA Graduate Student Researchers Program, and the Propulsion Research Center at Marshall Space Flight Center. The authors express thanks to Dr. George R. Schmidt, Mr. James J. Martin, Mr. Harold P. Gerrish, and Dr. Raymond A. Lewis for their assistance. Additional help from Dr. Robert E. Peterkin at the Air Force Research Laboratory is also appreciated.

REFERENCES

[1] Hill, P. G. and C. R. Peterson. Mechanics and Thermodynamics of Propulsion. Reading: Addison-Wesley, 1992.

[2] Kammash, T. and Flippo, K., "A Field Reversed Gasdynamic Mirror Fusion Propulsion System," STAIF AIP Conference Proceedings 458 v2 (1999), 1339.

[3] Schmidt, G. R., Gerrish, H. P., et al, "Antimatter Requirements and Energy Costs for Near-Term Propulsion Applications," J. Propulsion and Power v16 n5 (2000), 923.

[4] Frisbee, R. H. Interstellar Mission Propulsion Studies Status Update. Tenth Annual NASA/JPL/MSFC/AIAA Advanced Propulsion Research Workshop, April 1999.

[5] Gaidos, G., Lewis, R.A., et al. "Antiproton-Catalyzed Microfission/Fusion Propulsion Systems for Exploration of the Outer Solar System and Beyond," AIP 420 (1998), 1365.

[6] Gaidos, G., Lewis, R.A., et al. "AIMStar: Antimatter Initiated Microfusion for Pre-cursor Interstellar Missions," STAIF AIP Conference Proceedings, 458 (1999), 954.

[7] Meyer, K. J., "Payload Design for Project AIMStar: Antimatter Initiated Microfusion Starship," Senior Thesis, Dept. Aerospace Engineering, Pennsylvania State University, 1998.

[8] Tinkle, M.D., et al. "Modes of Spheriodal Ion Plasmas at the Brillouin Limit," AIP Conference Proceedings 331, AIP Publishing, 1995.

[9] Holzscheiter, M.H., et al, Phys. Lett A214, 279, 1996.

[10] "SRIM: The Stopping and Range of Ions in Matter," http://www.physics.isu.edu/ sigmabase/documents/ trim_manual.html. Updated 20 Dec 1995.

[11] Peterkin, R. E. and M. H. Frese. MACH: A Reference Manual. 1st ed. Air Force Research Laboratory: Philips Research Site, 1998.

[12] Gerwin, R. A., Marklin, G. J., et al, "Characterization of Plasma Flow Through Magnetic Nozzles," Los Alamos National Laboratory, LA-UR-89-4212.

[13] Sutton, G. Engineering Magnetohydrodynamics. New York: McGraw Hill, 1965.

[14] Ilin, A.V., et al. "Monte Carlo Particle Dynamics in a Variable Specific Impulse Magnetoplasma Rocket," Advanced Space Propulsion Laboratory, Johnson Space Center, 1998.